Iron enhances hepatic fibrogenesis and activates TGF-β signaling in murine hepatic stellate cells

Mehta, K.J., Coombes, J.D., Briones-Orta, M., Manka, P.P., Williams, R., Patel, V.B. and Sin, W.-K.

Iron enhances hepatic fibrogenesis and activates TGF-β signaling in murine hepatic stellate cells

Kosha J. Mehta[1, 2], Jason D. Coombes[1] , Marco Briones-Orta[1], Paul P. Manka[1, 3], Roger Williams[1], Vinood B. Patel[2] , Wing-Kin Syn[1, 4, 5,*]

[1]The Institute of Hepatology, Foundation for Liver Research, Faculty of Life Sciences and Medicine, King's College London UK.

[2]Department of Biomedical Sciences, University of Westminster, London, UK.

[3]Division of Gastroenterology and Hepatology, University Hospital Essen, Essen, Germany.

[4]Section of Gastroenterology, Ralph H Johnson VAMC, Charleston, South Carolina USA.

[5]Division of Gastroenterology and Hepatology, Department of Medicine, Medical University of South Carolina, Charleston, South Carolina, USA.

*Correspondence

Wing-Kin Syn, MD

Medical University of South Carolina

Strom Thurmond Building

114 Doughty Street

MSC 702, Room 402

Charleston SC 29425

USA

Office: 001-(843) 792-2301; Fax: 001- (843) 876-7232; Email: synw@musc.edu

Running title: Effect of iron on liver fibrogenesis

Conflict of interest: The authors declare no conflict of interest.

Funding: Foundation for Liver Research (WKS), Polkemmet Trust (WKS), Dunse Foundation / British Liver Trust (WKS).

Acknowledgements: GRX was kindly provided by Professor J Oliveira (Brazil).

List of Abbreviations:

ALD Alcoholic liver disease

DFO Deferoxamine

ECM Extracellular matrix

Holo-TfHolotransferrin

HSC Hepatic stellate cells

NAFLD Non-alcoholic fatty liver disease

NASH Non-alcoholic steatohepatitis

ROS Reactive oxygen species

TfR1 Transferrin receptor-1

TGF-β Transforming growth factor-beta

α-SMAAlpha smooth muscle actin

Abstract

Introduction:

Although excess iron induces oxidative stress in theliver, it is unclear whether it directly activates the hepatic stellate cells (HSC).

Methods:

Westudied theeffects of excess iron on fibrogenesis and TGF-β signaling in murine HSC. Cells were treated with holotransferrin (0.005-5 g/L) for 24 h, with or without the iron chelator deferoxamine (10 µM). Gene expressions (*α-SMA*, *Col1-α1*, *Serpine-1*, *TGF-β*, *Hif1-α,Tfrc* and *Slc40a1*) were analyzed by qRT-PCR, while the proteins TfR1, ferroportin, ferritin, vimentin, collagen, TGF-β RII and phospho-Smad2were examined by immunofluorescence, western blot and ELISA.

Results:

HSC expressed the iron-uptake protein TfR1, and the iron-exporter protein ferroportin. Holotransferrin up-regulated TfR1 expression by 1.8-fold ($p<0.03$) and ferritin accumulation (iron storage) by 2-fold ($p<0.01$). It increased HSC activation with 2-fold elevations ($p<0.03$) in*α-SMA* mRNA and collagen secretion, and a 1.6-fold increase ($p<0.01$) in vimentin protein. Moreover, holotransferrin activated the TGF-β pathway with *TGF-β* mRNA elevated 1.6-fold ($p=0.05$), and the proteins TGF-β RII and phospho-Smad2 elevated by 1.8-fold ($p<0.01$) and 1.6-fold ($p<0.01$), respectively.In contrast, iron chelation reduced ferritin levels by 30% ($p<0.03$), inhibited collagen secretion by up to 60% ($p<0.01$), reduced the expression of fibrogenic genes *α-SMA* (0.2-fold; $p<0.05$) and *TGF-β* (0.4-fold; $p<0.01$), and repressed the proteinsTGF-β RII and phospho-Smad2.

Conclusion:

HSC expressedthe iron transport proteins. Iron enhanced fibrogenesis and activated the TGF-β pathway, while iron chelation caused reversal, proposing this as a useful adjunctive therapy for fibrosis patients.Further studies in primary human HSC and animal models are necessary to confirm this.

Keywords: Fibrosis, Fibroblasts, Holotransferrin, Liver

Introduction

Chronic liver injury activates the hepatic stellate cells (HSC) and is characterized by upregulationof the HSC activation marker alpha smooth muscle actin (α-SMA), and increased expression of profibrogenic cytokines such as transforming growth factor-β (TGF-β). This invariably elevates the mesenchymal marker vimentin, anddeposition of extracellular matrix (ECM) components such as collagen to form a scar tissue, clinically referred as fibrosis. Fibrosis reversibility is possible during the early stage of the disease, but it is less likely when scar tissues undergo cross-linking and become mature (i.e. advanced

fibrosis)(1,2). Therefore, targeting fibrosis during the early stagesmay halt the progression of fibrosis to cirrhosis and mediate reversion, as seen in some studies. However, despite the promising advances in the reversion of fibrosis and even cirrhosis to some extent in human (3–5) and in animal models(6,7), mortality due to liver cirrhosis has doubled in the last 25 years. Liver transplantation remains the only curative option for end-stage cirrhosis and approximately 60% of liver transplantations are performed because of cirrhosis (8). Thus, further understanding of fibrogenic mechanisms is essential to help decelerate disease progression and increase the probability of regression.

Fibrosis-promoting chronic liver injury, as seen in viral hepatitis, alcoholic liver disease (ALD) and non-alcoholic fatty liver disease (NAFLD), often exhibits increased iron loading and de-regulated iron metabolism despite the differences in pathophysiology(9–13). Unlike hereditary hemochromatosis where specific mutations in iron-related genes lead to excessive intestinal iron and systemic and cellular iron overload (14), in the aforementioned etiologies, it remains unclear whether excess iron is a stimulator, mediator or simply a marker of advanced liver fibrosis.Under physiological conditions, iron is bound to its carrier protein transferrin, which delivers iron tothecells by binding to the iron–uptake protein transferrin receptor (TfR)1 expressed on cell surfaces.Conversely, cellular iron-efflux is mediated via the iron-exporter protein ferroportin and excess iron is stored as ferritin. During iron-loaded conditions, as observed in the aforementioned etiologies, when the buffering capacities of the iron-binding proteins transferrin and ferritin are saturated,the excess ‘free’, unbound, unquenchable iron accelerates the formation of reactive oxygen species (ROS) in the hepatocytes via the Fenton reaction, resulting in oxidative stress and hepatocyte injury(15,16). In turn, the damaged hepatocytes secrete cytokines and growth factors which activate the HSC and promote fibrogenesis (17,18). However, apart from these indirect effects of iron-induced hepatocyte-mediated oxidative stress, whether iron can

directly activate HSC fibrogenesis is unknown. No study has yet reported whether iron can directly modulate the HSC phenotype in murine HSCas far as we know.

Hence, in the present study, we hypothesized that iron can directly regulate the HSC phenotype.Accordingly, murine HSC were treated with holotransferrin (holo-Tf). Unlike previous studies that used inorganic sources of iron such as ferric chloride or ferric chloride: citrate for treatment of rat HSC (19,20), we used holo-Tf because it is the most relevant physiological form of iron. First, preliminary experiments involving time response studies (supplementary Fig.1 online) were conducted with holo-Tf. Based on these results, cells were treated with a wide rangeof holo-Tf concentrations (0.005 to 5 g/L) for 24 h and various parameters were assessed such as the expression of core fibrogenic genes and proteins by qRT-PCR and western blot and measurement of secreted collagen in cell-conditioned media. Further on, holo-Tf-induced activation of the TGF-β pathway was examined. Thereafter, we examined whether iron chelation via the iron chelator deferoxamine (DFO) could reduce the iron-induced fibrogenic effects. For this examination, cells were treated with a wide range of DFO concentrations (0.1 to 100 μM) for 24 h and parameterswere assessed thereafter. In another set of experiments, cells were treated with a combination of DFO and either 0.05 g/L, 0.5 g/L or 2 g/L holo-Tf for 24 h and then,the parameters were assessed. In the final set of experiments, first the cells were treated with holo-Tf for 24 h. Then, cells in each holo-Tf concentration were treated with 10 μM DFO for 24 h and then again for further 24 h. Data revealed that iron enhanced fibrogenesis and activated the TGF-β pathway, while iron chelation reversed fibrogenic responses and attenuated TGF-β signaling.

Materials and Methods

Cell culture and treatments

The mouse HSC line (GRX) was maintained in DMEM (Gibco, UK) with 2% fetal calf serum (FCS), 1% penicillin-streptomycin (Gibco, UK) and 1% gentamycin (Gibco, UK). Trypsinization was performed with Tryple-E solution (Gibco, UK). Cells were treated with holo-Tf (Sigma Aldrich, UK) (0, 0.005, 0.05, 0.5, 2 and 5 g/L) for 24 h and assessed for various parameters. In separate experiments, cells were treated with the iron chelator deferoxaminemesylate salt (DFO) (Sigma Aldrich, UK) (0, 0.1, 1, 10 and 100 µM) for 24 h and then harvested for assessments. In another set of experiments, referred to as the DFO

double dosage experiment, first, the cells were treated with 0, 0.05, 0.5 and 2 g/L holo-Tf for 24 h. Then, the cells were supplemented with 10 µM DFO for the next 24 h. Following this period, the cells were supplemented again with 10 µM DFO for further 24 h. At the end of the 72 h-treatment period, cells were harvested and the parameters were assessed. Gene expressions (*α-SMA*, *Col1-α1*, *Serpine-1*, *TGF-β*, *Hif1-α,Tfrc* and *Slc40a1*) were analyzed by qRT-PCR, while the proteins TfR1, ferroportin, ferritin, vimentin, collagen, TGF-β RII and phospho-Smad2 were examined by immunofluorescence, western blot and ELISA.

Immunofluorescence for iron-transport proteins

The cellular iron-uptake protein TfR1 and the iron-export protein ferroportin were detected by immunofluorescence. Briefly, cells were fixed in 4 % formaldehyde for 10 min at room temperature, blocked with 1% BSA in 0.1% PBS-tween, and then probed with rabbit anti-TfR1 antibody (5 µg/mL, Abcam AB84036) or rabbit anti-ferroportin antibody (10 µg/mL, Abcam, AB85370), as per manufacturer's instructions. Fluorescence detection was achieved by using a secondary goat anti-Rabbit Alexa Fluor® 488 antibody (2 µg/mL, Abcam).

Gene expression analysis

Cells were washed with PBS, treated with TRI reagent (Sigma Aldrich, UK) (500 µL per well) and the RNA was extracted as per manufacturer's instructions. cDNA synthesis of 1000 ng RNA was conducted using iScript cDNA Synthesis Kit (Biorad, UK), as recommended by the manufacturer. The mRNA expressions of the genes *Serpine-1*, *Col1-α1*, *α-SMA*, *TGF-β* and *Hif1-α* were normalized to *s9* expression (supplementary table S1 online) (21,22). Gene expression was measured using Applied

Biosystems 7500 and the data was analyzed by the relative quantification method, Delta-Delta Ct (ΔΔCt) and expressed as $2^{-\Delta\Delta Ct}$(23).

Ferritin level measurements

Cells were washed with PBS and lysed with lysis buffer [RIPA buffer (Sigma- Aldrich, UK) and Complete-Miniprotease inhibitor cocktail tablet (Roche, UK)], as per manufacturer's instructions. Samples were collected on ice, vortexed for 3 sec and ferritin levels were measuredusing a mouse ferritin ELISA kit (Abcam, UK). Levels were normalized to protein concentration measured by Precision Red (Cyclosystem, USA).

Western blot

Cells were washed with PBS and lysed with RIPA buffer (Sigma-Aldrich, UK) containing Complete-Mini Protease inhibitor cocktail (Roche, UK) and Phospho-stop (Roche, UK), as per manufacturer's instructions. Cell extracts were centrifuged for 5 min at 14,000 rotations/minute and the supernatant was electrophoresed on Novex Blot 4-12 % Bis-Tris gels as per the Novex Bolt system (ThermoFisher Scientific, UK). Following protein transfer to PVDF or nitrocellulose membrane via the iBlot system (Invitrogen, UK), membranes were probed with primary antibodies (1:1000) overnight in a cold room, followed by treatment with appropriate HRP-conjugated detection antibodies (1:10,000) for 1 h, at RT on shaker (Supplementary table 2 online). Protein bands were observed on the ChemiDoc imager (Biorad, UK) and analyzed using the Image lab software (Bio-Rad, UK). Protein density was analyzed by the Image-J software available at the National Institutes of Health.

Viability Assay and Collagen secretion

For viability studies, cells were first seeded at a density of 5 $X10^3$ cells/well in 96-well plates. After 24 h treatment with holo-Tf, viability was measured by using the CCK-8 kit (Dojindo Laboratories, Japan), as per the manufacturer's instructions. Secreted collagen was measured in cell-conditioned media. Cells were first seeded in a 6-well plate. Following holo-Tftreatments, conditioned media werecollected and collagen was measured via the Sircol assay (Bicolor, UK), as per the manufacturer's protocol. Levels were normalized to protein concentration measured by Precision Red (Cyclosystem, USA).

Statistical analysis

Data was analyzed using student's T-test (two-tailed distribution, two sample, and unequal variance). The level of significance was set at $p<0.05$. Data was presented as mean ± SD (n=3-9) and statistical analyses are based on n values.

Results

HSC expressed iron transport proteins and responded to exogenous iron

The HSC expressed the cellular iron-uptake protein TfR1 (Fig.1a), and the iron-export protein ferroportin (Fig.1b). Basal mRNA expression of the core fibrogenic genes *Serpine-1*, *Col1-α1* and *α-SMA*, and the key iron transport genes *Tfrc*and *Slc40a1* in the HSC are shown (Fig.1c).To assess whether theHSC would respond to exogenous iron, cells were treated with holo-Tf, the physiological relevant form of iron. Data showed thatholo-Tf significantly upregulated the expression of the iron-uptake protein TfR1 (holo-Tf 0.05 g/L: 1.7-fold, $p<0.03$; holo-Tf 0.5 g/L: 1.8-fold, $p<0.03$; holo-Tf 2 g/L: 1.7-fold, $p<0.05$) (Fig.1d). As the greatest induction of fibrogenic genes *Serpine-1* and *α-SMA* occurred 24 h post-treatment (supplementary Fig.1 online), the HSC were treated with holo-Tf for 24 h in all subsequent experiments.

To determine whether holo-Tf treatmentled to accumulation of cellular iron, we measured the levels of the iron-storage protein ferritin. Results revealed that holo-Tf caused a dose-dependent accumulation of cellular iron: treatment with 0.005 g/L of holo-Tf increased ferritin by 1.6-fold ($p<0.01$), and treatment with 5 g/L of holo-Tf increased ferritin by 2-fold ($p<0.01$) (Fig.1e).

Holo-Tf activated HSC and induced deposition of the extracellular matrix collagen

As HSC expressed the iron transport proteins and responded to exogenous iron by increasing cellular iron (Figs.1aand 1e),we examined whether this iron accumulation was associated with HSC activation. Accordingly, theHSC were treated with holo-Tf for 24 h and then harvested for mRNA and protein analysis. Data revealed thatholo-Tf upregulated the HSC activation marker *α-SMA* by up to 2-fold ($p<0.03$) (Fig.2a), and the pro-fibrogenic marker and TGF-β target gene,*serpine-1*by up to 2.5-fold ($p<0.05$) (Fig.2b).

Furthermore, holo-Tf treatment induced collagen secretion intothe conditioned media by up to 1.9-fold ($p<0.03$) (Fig.2c) along with increased expression of the protein vimentin by up to 1.6-fold ($p<0.01$)upon 0.5 g/L holo-Tf treatment(Fig.2d and supplementary Fig.2 online). Previous studies reported that iron could mediate its effects via the hypoxia-inducible factor 1, alpha subunit (HIF-1 α) (24). Here, holo-Tf increased Hif-1 α expression by up to 1.9-fold ($p<0.05$) after a 24 h treatment (supplementary Fig.2 online). The addition of holo-Tf had no effect on HSC viability (supplementary Fig.2 online).

Holo-Tf upregulated TGF-β mRNA and promoted TGF-βsignaling

The fibrotic liver microenvironment is enriched with pro-fibrogenic factors (25). As TGF-β is the prototypical pro-fibrogenic cytokine and is over expressed in the fibrotic liver tissue(26), we examined whether holo-Tf enhanced TGF-β signaling. Data showed that holo-Tf upregulated TGF-β mRNA expression (holo-Tf0.005 g/L: 1.2-fold, p=0.05; holo-Tf0.05 g/L: 1.7-fold, p=0.07; holo-Tf0.5 g/L: 1.6-fold, p=0.05) (Fig.3a).Holo-Tf also increased protein levels of the TGF-β receptor TGF-β RII by up to 1.8-fold (p< 0.01) (Fig.3b) and phospho-Smad 2 by up to 1.6-fold (p<0.01) (Fig.3c).Collectively, the data indicated that holo-Tf directly activatedthe HSC via the canonical TGF-β signaling.

Iron chelation abrogated iron-induced fibrogenesis and inhibited TGF-β signaling

DFO treatment has been successfully used on hemochromatosis (iron overload) patients that are unable to undergo phlebotomy (27). Following the confirmation that exogenous iron could promote TGF-β signaling and activate the HSC (Figs.2 and 3), we aimed at examining whether iron depletion via DFO inhibited HSC activation.Accordingly, HSC were treated with a range of DFO concentrations for 24 h. Results showed significantly reduced ferritin levels (p<0.03) when treated with the lowest DFO concentration (0.1 μM) and this decrease was maintained across all other DFO concentrations (Fig.4a). In addition, there were significant reductions (p<0.05) in the mRNA expressions of *α-SMA*(Fig.4b), *TGF-β* (supplementary Fig.3 online), *Col1-α1*(Fig.4c), and in the levels of secreted collagen (Fig.4d).

Next, we aimed tounderstand whether DFO inhibited the holo-Tf-induced HSC fibrogenesis. Based on the results of the iron-chelation experiments (Fig.4 and supplementary Fig.3 online), cells were initially treated with a combination of 10 μM DFO with each concentration of holo-Tf (0.05, 0.5 and 2 g/L) for 24 h. The choice of 10 μM concentration of DFO was based on the DFO-only treatments where this was the lowest concentration that significantly reduced collagen mRNA and protein secretion (Figs. 4c and

4d). Results showed no significant alteration in responses (supplementary Fig.4 online). Therefore, we conducted the DFO-double dosage experiment, as explained in the Methods. Briefly, the cells were first treated with holo-Tf for 24 h, then supplemented with 10 µM DFO, twice for 24 h each and then harvested after the 72 h treatment period. For the DFO-double dosage treatment, we excluded the lowest and the highest dosages of 0.005 g/L and 5 g/L holo-Tf, respectively. This is because these are physiologically less relevant, and the holo-Tf concentration range from 0.05 to 2 g/L would more closely represent the low-to moderate iron excess conditions, as observed in several non-hereditary iron-loaded conditions such as ALD and viral hepatitis.

Results showed that ferritin levels significantly reduced by 30% ($p<0.03$) (Fig.5a). Holo-Tf-induced collagen secretion was also reduced by up to 60 % ($p<0.01$) (Fig.5b). Moreover, the mRNA expressions of *α-SMA* and *Col1-α1*were significantly repressed by up to 80% ($p<0.05$) and 30% ($p<0.03$), respectively (Figs.5c and 5d). Similarly,the mRNA expressions of *TGF-β* and *Hif1-α* were significantly down regulated by up to 60% ($p<0.01$) and 50% ($p<0.03$), respectively (supplementary Fig.5 online). The DFO double dosage treatment also decreased the iron-induced levels of theTGF-βpathway proteinsTGF-β RII (Fig.6a) and phospho-Smad2 (Fig.6b).

Discussion

The role of iron in causing hepatocyte-mediated damage to the liver and thereby contribute in the progression of fibrosis is already established(18). However, the direct role of iron in the activation of HSC, the principle cells that orchestrate fibrosis, has not been investigated before. Hence, thepresent study aimed to understand the direct effect of iron on HSC activation and examine the putative mechanism that may mediate this process.As hypothesized, results showed that iron enhanced fibrogenesis and activated TGF-β signaling,while iron chelation caused reversal.

Firstly, the presence of the iron uptake protein TfR1 and the iron storage protein ferritin in the murine HSC was ascertained (Figs. 1a and 1b). Then, unlike previous studies (19,20,28), we confirmed holo-Tf-induced intracellular iron accumulation (ferritin levels), in addition to DFO-mediated reduction in cellular

iron under basal and holo-Tf supplemented conditions (Figs. 1e, 4a and 5a). Thus, the reported alterations in fibrosis and TGF-β-pathway-related genes and proteins could be attributed to holo-Tf treatment and cellular iron accumulation and chelation. The saturation of ferritin levels (iron accumulation) upon holo-Tf treatment (Fig. 1e) could be due two reasons; first, the saturation of transferrin receptors on cell surfaces with holo-Tf, which may have prevented further iron uptake, and second, the cellular iron regulatory mechanisms exhibited by the iron response elements on *Tfrc* transcripts, that prevent its translation to TfR1 protein under intracellular iron–replete state. This in turn would limit cellular iron acquisition due to reduction in transferrin-receptors on the cell surfaces (29).

Compared with previous elegant iron-related studies in HSC (19,20,28), we examined a widerrange of fibrosis-associated genes and proteins such as *α-SMA*, *Col1-α1*, *Serpine-1*, *Hif1-α*, vimentin and collagen under a wider range of concentrations of holo-Tf and DFO to obtain a better insight into iron-induced fibrogenic mechanisms. Data showed that iron treatment, followed by iron acquisition directly activated the HSC and enhanced fibrogenesis (Figs.2a and 2c). The upregulation of *α-SMA* (Fig.2a) is consistent with previous studies where transferrin increased the expression of α-SMA protein in rat HSC (28). Increases in collagen secretion and vimentin protein expression provided further evidence that iron enhancedthe levels of fibrosis-associated proteins (Figs.2c and 2d).

Moreover, unlike other studies, we examined the possible underlying mechanism by which iron may induce the fibrogenic responses. Data showed that holo-Tf enhanced TGF-β signaling (Fig.3), which is known to regulate the expressions of pro-fibrogenic genes and ECM deposition (30). This holo-Tf-induced activation of the TGF-β signaling pathway through upregulation of *TGF-β* mRNA and increased expression of the TGF-β pathway proteins, TGF-β RII and phospho-Smad2 (Fig.3) is novel and has not

been shown before, as far as we know. Collectively, the data indicates thatthe iron-induced fibrogenesis could be mediated, in part, by the activation of the TGF-β pathway (Fig.3 and Fig.6).Thus, the canonical free-iron mediated oxidative stress, together with the direct stimulation of fibrogenic responses by iron, can amplify tissue injury and accelerate fibrosis progression in chronic iron-excess pathologies.

Conversely, iron chelation repressed the iron-induced fibrogenesis and attenuated TGF-β signaling (Figs.5 and 6), thereby reiterating the involvement of iron in fibrogenesis and TGF-β signaling. Distinct from previous studies where DFO-mediated reduction in procollagen and α-SMA was observed under basal conditions (without holo-Tf treatment) (19), we observed that DFO suppressed fibrotic responses under iron excess conditions (after holo-Tf treatment) (Fig.5 and supplementary Fig.5 online). Thus, while it is already established that iron chelation removes excess iron and reduces the excess-iron-mediated oxidative stress (31), the present study showed that it can inhibit iron-induced fibrotic responses (Figs.5 and 6). This can be of great clinical value in halting fibrosis progression, particularly in conditions of low to moderate iron overload such as in ALD, NAFLD, and NASH, where iron-removal via phlebotomy may not be an appropriate option, unlike hereditary haemochromatosis where iron-removal via phlebotomy is a standard practice (14,32). Thus, iron chelation may be directly anti-fibrotic and could be a useful adjunct therapy to reduce fibrotic injury in patients with liver fibrosis.

Interestingly, following the DFO double dosage treatment, collagen protein reduced under all concentrations of holo-Tf (Fig.5b), while its mRNA expression reduced only for low iron conditions of 0.05 g/L (Fig.5d). While this partly indicates the diminishing effect of DFO on collagen mRNA expression under high iron conditions, it also suggests a probable lag phase between the mRNA and protein expression. Slow responses of *col1α1* mRNA responses have been observed in previous

studies where its expression increased only by 1.5-fold after a long 48 h incubation with 0.2 g/L iron treatment (28). Also, in another study, procollagen mRNA expression was maximum at the low concentration of 5 μM iron and induced a lower increase at higher doses of 10 and 25 μM iron (20). In yet another study, the inhibition of α2 (I) collagen by DFO was observed after 96 hours or 7 days (19). In this light, it is probable that increasing the duration of the DFO treatment beyond the double dosage treatment (48 h) to 96 h or beyond may demonstrate similarity between the mRNA and protein responses. Moreover, it is probable that DFO may have an immediate effect on collagen protein secretion rather than mRNA expression, as observed here. Further studies would be required to clarify this.

Lastly, we also attempted to understand the link between hypoxia, iron and fibrosis. Hypoxia has been implicated in the development of several liver diseases because the gradient of oxygen through the hepatic lobule greatly affects the functions of the hepatic cells (24). While hypoxia modulates iron homeostasis through hypoxia inducible factors (HIFs) (24,29,33), several fibrosis-associated HIF-target genes have been identified, such as *serpine-1* and *prolyl-4 hydroxylase α2* (34), suggesting a link between iron homeostasis and fibrosis via HIFs. Predictably, HIF-1α has been shown to enhance fibrogenic responses (34–36). The present study demonstrated an upregulation of *Hif-1α* mRNA upon holo-Tf treatments, followed by its repression upon DFO treatment (Supplementary Figs. 2 and 5 online), which suggests that the anti-fibrotic effect of DFO may be through the modulation of HIF-1α. More studies should be conducted to identify additional HIF-regulated fibrogenic and iron-related genes that could be developed as targets for anti-fibrotic therapies.

In this study, cells were treated with a wide range of holo-Tf concentration (from 0.005 to 5 g/L) to enable the inclusion of the normal physiological range (2-3 g/L) and the different ranges of iron-loaded transferrin observed in pathological conditions like iron deficiency and iron overload. Assuming the approximate average of 30% iron saturation for 2 g/L transferrin accounts to 0.6 g/L of iron-loaded transferrin, whereas a 45 -50% iron-saturated transferrin, as in case of hemochromatosis, accounts to 1.4 -1.5 g/L of iron-loaded transferrin. Thus, the chosen concentrations covered the range from 0.6 to 2 g/L of iron-loaded transferrin. We anticipated that the high 5 g/L concentration might cause saturation of system and lead to outlier responses. However, inclusion of this concentration in our experimental design was necessary to provide evidence of this. For example, holo-Tf-induced elevations in TfR1 (Fig.1D), vimentin (Fig.2d), TGF-β RII (Fig.3b), and psmad-2 (Fig.3c) were observed only up to 2 g/L holo-Tf treatment, whereas upon 5 g/L treatment, the responses reduced in comparison to 2 g/L treatment. In addition, the lower-end concentrations of 0.05 and 0.005 g/L were chosen to observe a clear gradient in responses if any and to accommodate fold differences in treatment concentrations so that the responses could be interpreted accordingly.

Further studies in primary human hepatocytes and in animal models of liver fibrosis are needed to confirm these DFO-mediated anti-fibrotic effects. Such studies are promising because previous studies have shown the beneficial effects of DFO such as in reducing inflammation and atherosclerosis in mice models (37). Subsequently, clinical trials can be conducted on ALD, NAFLD and /or NASH patients with different stages of liver fibrosis and the antifibrotic effects of iron-chelation can be evaluated by measuring the levels of fibrotic markers in these patients. In addition, DFO can be used in a synergistic combination with another iron chelator deferriprone in hepatic cells and animal models to examine their combined antifibrotic effect. Such combinations have shown a promising potential in reducing

intracellular iron pool and transferrin saturation(38,39)and may thereby help in formulating effective treatment strategies for patients that reduce dosage and minimize the side effects.

Conclusion

We confirmed a direct connection between iron and fibrosis. Data showedthat iron can directly activate the TGF-β pathway and directly promote fibrosis,while chelation of iron by usingDFO can reverse this by inhibiting TGF-β signaling and repressing fibrogenesis. Therefore, iron chelation may be a useful adjunctive therapy to decelerate fibrosis progression. Further studies in primary human HSC and animal models of liver fibrosis will be needed to confirm these benefits.

References

1. Moreira RK. Hepatic stellate cells and liver fibrosis. Arch Pathol Lab Med. 2007 Nov;131(11):1728–34.
2. Li D, Friedman SL. Liver fibrogenesis and the role of hepatic stellate cells: new insights and prospects for therapy. J Gastroenterol Hepatol. 1999 Jul;14(7):618–33.
3. D'Ambrosio R, Aghemo A, Rumi MG, Ronchi G, Donato MF, Paradis V, et al. A morphometric and immunohistochemical study to assess the benefit of a sustained virological response in hepatitis C virus patients with cirrhosis. Hepatol Baltim Md. 2012 Aug;56(2):532–43.
4. McPherson S, Hardy T, Henderson E, Burt AD, Day CP, Anstee QM. Evidence of NAFLD progression from steatosis to fibrosing-steatohepatitis using paired biopsies: implications for prognosis and clinical management. J Hepatol. 2015 May;62(5):1148–55.
5. Marcellin P, Gane E, Buti M, Afdhal N, Sievert W, Jacobson IM, et al. Regression of cirrhosis during treatment with tenofovir disoproxil fumarate for chronic hepatitis B: a 5-year open-label follow-up study. The Lancet. 2013 Feb 9;381(9865):468–75.
6. Sobrevals L, Rodriguez C, Romero-Trevejo JL, Gondi G, Monreal I, Pañeda A, et al. Insulin-like growth factor I gene transfer to cirrhotic liver induces fibrolysis and reduces fibrogenesis leading to cirrhosis reversion in rats. Hepatol Baltim Md. 2010 Mar;51(3):912–21.
7. Kisseleva T, Cong M, Paik Y, Scholten D, Jiang C, Benner C, et al. Myofibroblasts revert to an inactive phenotype during regression of liver fibrosis. Proc Natl Acad Sci. 2012 Jun 12;109(24):9448–53.
8. Manns MP. Liver cirrhosis, transplantation and organ shortage. Dtsch Arzteblatt Int. 2013 Feb;110(6):83–4.

9. Milic S, Mikolasevic I, Orlic L, Devcic E, Starcevic-Cizmarevic N, Stimac D, et al. The Role of Iron and Iron Overload in Chronic Liver Disease. Med Sci Monit Int Med J Exp Clin Res. 2016 Jun 22;22:2144–51.

10. Fujita N, Takei Y. Iron overload in nonalcoholic steatohepatitis. Adv Clin Chem. 2011;55:105–32.

11. Nelson JE, Klintworth H, Kowdley KV. Iron metabolism in Nonalcoholic Fatty Liver Disease. Curr Gastroenterol Rep. 2012 Feb;14(1):8–16.

12. Sebastiani G, Tempesta D, Alberti A. Hepatic iron overload is common in chronic hepatitis B and is more severe in patients coinfected with hepatitis D virus. J Viral Hepat. 2012 Feb;19(2):e170-176.

13. Rouault TA. Hepatic iron overload in alcoholic liver disease: why does it occur and what is its role in pathogenesis? Alcohol Fayettev N. 2003 Jun;30(2):103–6.

14. Pietrangelo A. Hereditary hemochromatosis: pathogenesis, diagnosis, and treatment. Gastroenterology. 2010 Aug;139(2):393–408, 408.e1-2.

15. Pietrangelo A. Metals, oxidative stress, and hepatic fibrogenesis. Semin Liver Dis. 1996 Feb;16(1):13–30.

16. Lemire JA, Harrison JJ, Turner RJ. Antimicrobial activity of metals: mechanisms, molecular targets and applications. Nat Rev Microbiol. 2013 Jun 1;11(6):371–84.

17. Faouzi S, Lepreux S, Bedin C, Dubuisson L, Balabaud C, Bioulac-Sage P, et al. Activation of cultured rat hepatic stellate cells by tumoral hepatocytes. Lab Investig J Tech Methods Pathol. 1999 Apr;79(4):485–93.

18. Philippe M-A, Ruddell R-G, Ramm G-A. Role of iron in hepatic fibrosis: one piece in the puzzle. World J Gastroenterol. 2007 Sep 21;13(35):4746–54.

19. Jin H, Terai S, Sakaida I. The iron chelator deferoxamine causes activated hepatic stellate cells to become quiescent and to undergo apoptosis. J Gastroenterol. 2007 Jun 29;42(6):475–84.

20. Gardi C, Arezzini B, Fortino V, Comporti M. Effect of free iron on collagen synthesis, cell proliferation and MMP-2 expression in rat hepatic stellate cells. Biochem Pharmacol. 2002 Oct 1;64(7):1139–45.

21. Coombes JD, Swiderska-Syn M, Dollé L, Reid D, Eksteen B, Claridge L, et al. Osteopontin neutralisation abrogates the liver progenitor cell response and fibrogenesis in mice. Gut. 2015 Jul;64(7):1120–31.

22. Scotland PB, Heath JL, Conway AE, Porter NB, Armstrong MB, Walker JA, et al. The PICALM Protein Plays a Key Role in Iron Homeostasis and Cell Proliferation. PLoS ONE [Internet]. 2012 Aug 30 [cited 2016 Jun 30];7(8). Available from: http://www.ncbi.nlm.nih.gov/pmc/articles/PMC3431333/

23. Livak KJ, Schmittgen TD. Analysis of relative gene expression data using real-time quantitative PCR and the 2(-Delta Delta C(T)) Method. Methods San Diego Calif. 2001 Dec;25(4):402–8.

24. Peyssonnaux C, Nizet V, Johnson RS. Role of the hypoxia inducible factors HIF in iron metabolism. Cell Cycle Georget Tex. 2008 Jan 1;7(1):28–32.

25. Lee UE, Friedman SL. Mechanisms of Hepatic Fibrogenesis. Best Pract Res Clin Gastroenterol. 2011 Apr;25(2):195–206.

26. Dooley S, ten Dijke P. TGF-β in progression of liver disease. Cell Tissue Res. 2012 Jan;347(1):245–56.

27. Nielsen P, Fischer R, Buggisch P, Janka-Schaub G. Effective treatment of hereditary haemochromatosis with desferrioxamine in selected cases. Br J Haematol. 2003 Dec;123(5):952–3.

28. Bridle KR, Crawford DHG, Ramm GA. Identification and characterization of the hepatic stellate cell transferrin receptor. Am J Pathol. 2003 May;162(5):1661–7.

29. Muckenthaler MU, Galy B, Hentze MW. Systemic iron homeostasis and the iron-responsive element/iron-regulatory protein (IRE/IRP) regulatory network. Annu Rev Nutr. 2008;28:197–213.

30. Ranganathan P, Agrawal A, Bhushan R, Chavalmane AK, Kalathur RKR, Takahashi T, et al. Expression profiling of genes regulated by TGF-beta: Differential regulation in normal and tumour cells. BMC Genomics. 2007;8:98.

31. Jomova K, Valko M. Importance of iron chelation in free radical-induced oxidative stress and human disease. Curr Pharm Des. 2011;17(31):3460–73.

32. Bacon BR, Adams PC, Kowdley KV, Powell LW, Tavill AS, American Association for the Study of Liver Diseases. Diagnosis and management of hemochromatosis: 2011 practice guideline by the American Association for the Study of Liver Diseases. Hepatol Baltim Md. 2011 Jul;54(1):328–43.

33. Peyssonnaux C, Zinkernagel AS, Schuepbach RA, Rankin E, Vaulont S, Haase VH, et al. Regulation of iron homeostasis by the hypoxia-inducible transcription factors (HIFs). J Clin Invest. 2007 Jul;117(7):1926–32.

34. Halberg N, Khan T, Trujillo ME, Wernstedt-Asterholm I, Attie AD, Sherwani S, et al. Hypoxia-inducible factor 1alpha induces fibrosis and insulin resistance in white adipose tissue. Mol Cell Biol. 2009 Aug;29(16):4467–83.

35. Higgins DF, Kimura K, Bernhardt WM, Shrimanker N, Akai Y, Hohenstein B, et al. Hypoxia promotes fibrogenesis in vivo via HIF-1 stimulation of epithelial-to-mesenchymal transition. J Clin Invest. 2007 Dec;117(12):3810–20.

36. Moon J-O, Welch TP, Gonzalez FJ, Copple BL. Reduced liver fibrosis in hypoxia-inducible factor-1alpha-deficient mice. Am J Physiol Gastrointest Liver Physiol. 2009 Mar;296(3):G582-592.

37. Zhang W-J, Wei H, Frei B. The iron chelator, desferrioxamine, reduces inflammation and atherosclerotic lesion development in experimental mice. Exp Biol Med Maywood NJ. 2010 May;235(5):633–41.

38. Devanur LD, Evans RW, Evans PJ, Hider RC. Chelator-facilitated removal of iron from transferrin: relevance to combined chelation therapy. Biochem J. 2008 Jan 15;409(2):439–47.

39. Vlachodimitropoulou Koumoutsea E, Garbowski M, Porter J. Synergistic intracellular iron chelation combinations: mechanisms and conditions for optimizing iron mobilization. Br J Haematol. 2015 Sep;170(6):874–83.

Figure Legends

Fig.1 Expression of iron transport and storage proteins in murine HSC

The immunofluorescence images of (a) the iron importerprotein TfR1 and (b) the iron exporter ferroportin on murine HSC under basal conditions for 48 hhave been shown. (c) The cDNA amplicons obtained during qRT-PCR detectionof *Serpine-1, Col1-α1, α-SMA, Tfrc*, *Slc40a1* and the reference gene *s9*, respectively, under basal conditions for 48 h have been shown on 1% agarose gel. (d) Western blot detection of TfR1 following holo-Tf treatment for 24 h. (e) Detection of the iron storage protein ferritin by ELISA following holo-Tf treatment for 24 h (n=6-9). Data is presented as mean ± SD. *p<0.05, **p<0.03 and ***p<0.01 compared to basal conditions.

Fig.2 Exogenous iron activatedmurine HSC

The mRNA expressions of (a) *α-SMA*(n=5-9)and (b) *Serpine-1*(n=5-9) following holo-Tf treatments for 24 h have been shown. (c) Collagen secretion following holo-Tf treatment for 24 h, as measured by

Sircol assay(n=3-7). (d) Western blot detection of vimentin following holo-Tf treatment for 24 h. Data is presented as mean ± SD. *p<0.05 and **p<0.03 compared to basal conditions.

Fig.3 Iron loading activated the TGF-β pathway in murine HSC

(a) The mRNA expression of *TGF-β*(n=5-9)following holo-Tf treatment for 24 h. Representative images of the TGF-β pathway proteins (b)TGF-β RII (n=3) and (c) phospho-Smad 2(n=6), as detected by western blot following holo-Tf treatmentfor 24 h are shown. Data is presented as mean ± SD. *p<=0.05 and **p<0.03 compared to basal conditions.

Fig.4 Iron chelation repressed fibrotic responses in murine HSC

The figure depicts the parameters assessed following treatment of murine HSC with a range of DFO concentrations for 24 h. (a) Ferritin levelsdetected by ELISA (n=5-8), mRNA expressions of (b) *α-SMA*(n=4-7)and (c) *Col1-α1*(n=4-7), and (d) collagen secretionlevelsmeasured by Sircoll assay (n=3) have been shown. Data is presented as mean ± SD. *p<0.05 and **p<=0.03 compared to basal conditions.

Fig.5 Iron chelation reduced iron-induced ferritin levels and attenuated fibrotic responses in murine HSC

The figure depicts the parameters assessed following the DFO double dosage treatment (explained in Methods) in murine HSC. (a) Ferritin levels measured by ELISA(n=4), (b) collagen secretion measured by Sircol assay(n=4), and the mRNA expressions of (c) *α-SMA*(n=3)and (d) *Col1-α1*(n=3) have been shown. Data is presented as mean ± SD. *p<0.05, **p<0.03 and ***p<0.01 compared to basal conditions.

Fig.6 Iron chelation inhibited TGF-β signaling in murine HSC

The figure depictsthe proteins of the canonical TGF-β pathway in murine HSC followingtheDFO double dosage treatment, as explained in the Methods. (a) TGF-β RII and (b) phospho-Smad 2 detection by western blot have been shown.

Figures.

Fig.1

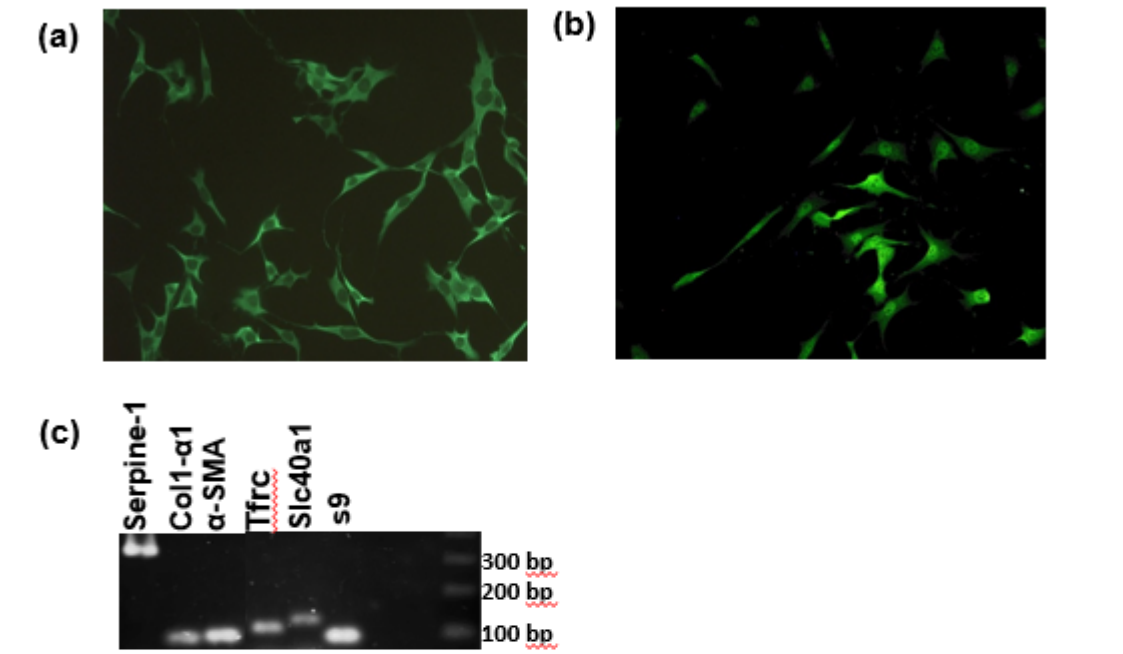
(a)
(b)
(c)
Serpine-1
Col1-α1
α-SMA
Tfrc
Slc40a1
s9
300 bp
200 bp
100 bp
(d)
Basal 0.005g/L 0.05g/L 0.5 g/L 2 g/L 5 g/L
TfR1
β-actin
TfR1/actin ratio
Basal 0.005g/L 0.05g/L 0.5g/L 2g/L 5g/L
Holo-Tf treatments
(e)
ng ferritin/ mg protein
Basal 0.005 g/L 0.05 g/L 0.5 g/L 2 g/L 5 g/L
Holo-Tf treatments for 24 h

Fig.2

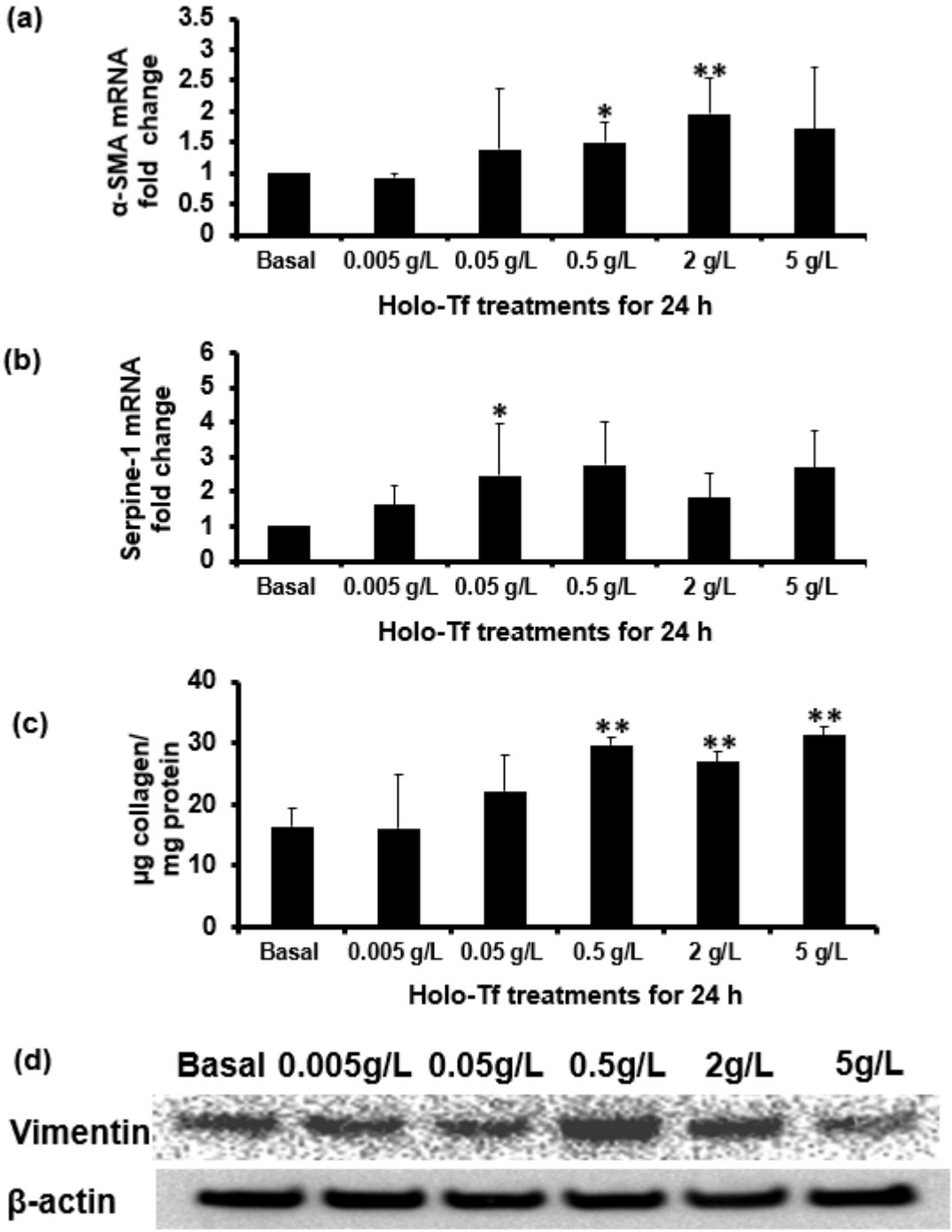
(a)
α-SMA mRNA fold change
3.5
3
2.5
2
1.5
1
0.5
0
*
**
Basal
0.005 g/L
0.05 g/L
0.5 g/L
2 g/L
5 g/L
Holo-Tf treatments for 24 h
(b)
Serpine-1 mRNA fold change
6
5
4
3
2
1
0
*
Basal
0.005 g/L
0.05 g/L
0.5 g/L
2 g/L
5 g/L
Holo-Tf treatments for 24 h
(c)
μg collagen/ mg protein
40
30
20
10
0
**
**
**
Basal
0.005 g/L
0.05 g/L
0.5 g/L
2 g/L
5 g/L
Holo-Tf treatments for 24 h
(d)
Basal
0.005g/L
0.05g/L
0.5g/L
2g/L
5g/L
Vimentin
β-actin

Fig.3

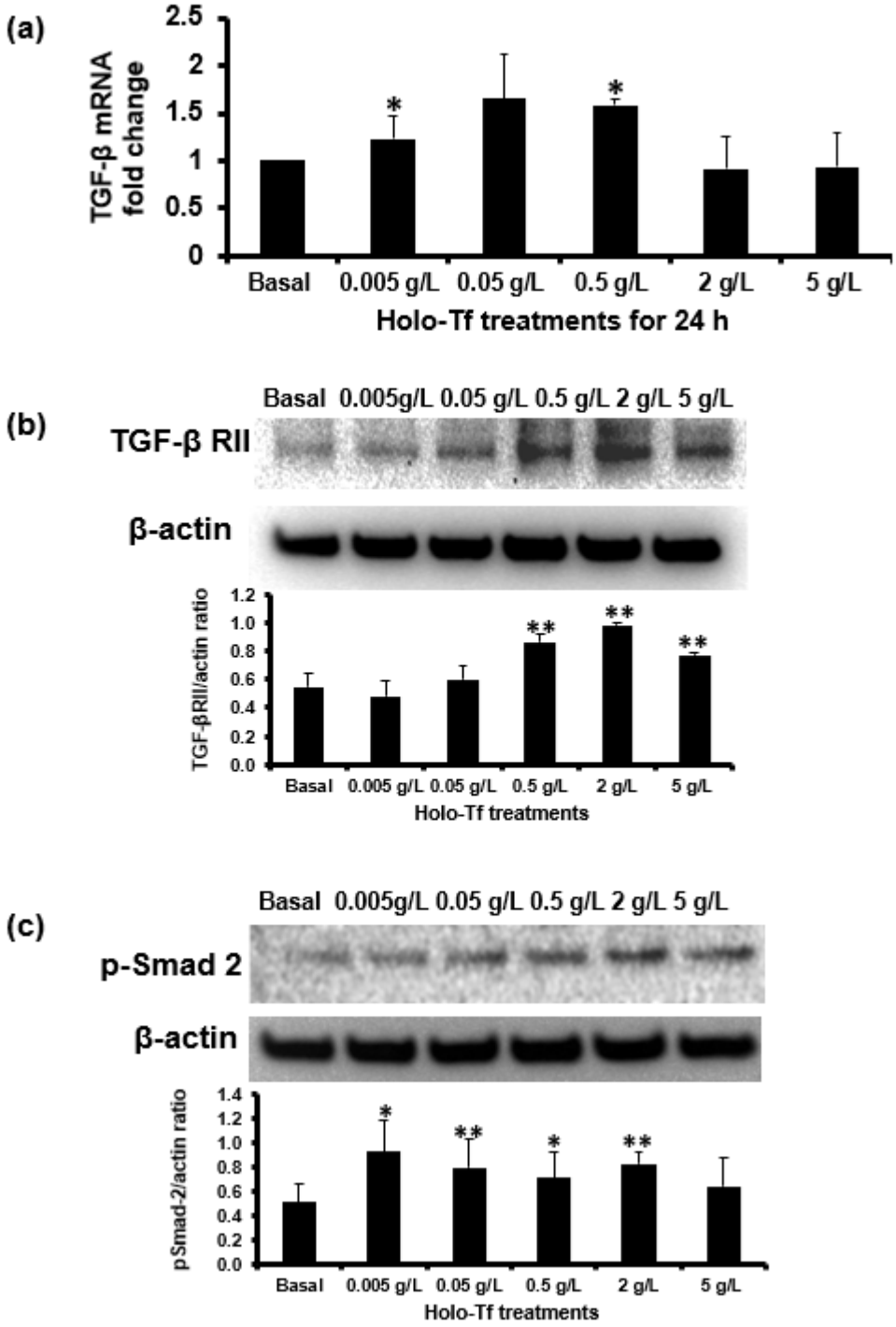
(a)
TGF-β mRNA fold change
2.5
2
1.5
1
0.5
0
*
*
Basal
0.005 g/L
0.05 g/L
0.5 g/L
2 g/L
5 g/L
Holo-Tf treatments for 24 h
(b)
Basal 0.005g/L 0.05 g/L 0.5 g/L 2 g/L 5 g/L
TGF-β RII
β-actin
TGF-βRII/actin ratio
1.2
1.0
0.8
0.6
0.4
0.2
0.0
**
**
**
Basal
0.005 g/L
0.05 g/L
0.5 g/L
2 g/L
5 g/L
Holo-Tf treatments
(c)
Basal 0.005g/L 0.05 g/L 0.5 g/L 2 g/L 5 g/L
p-Smad 2
β-actin
pSmad-2/actin ratio
1.4
1.2
1.0
0.8
0.6
0.4
0.2
0.0
*
**
*
**
Basal
0.005 g/L
0.05 g/L
0.5 g/L
2 g/L
5 g/L
Holo-Tf treatments

Fig.4

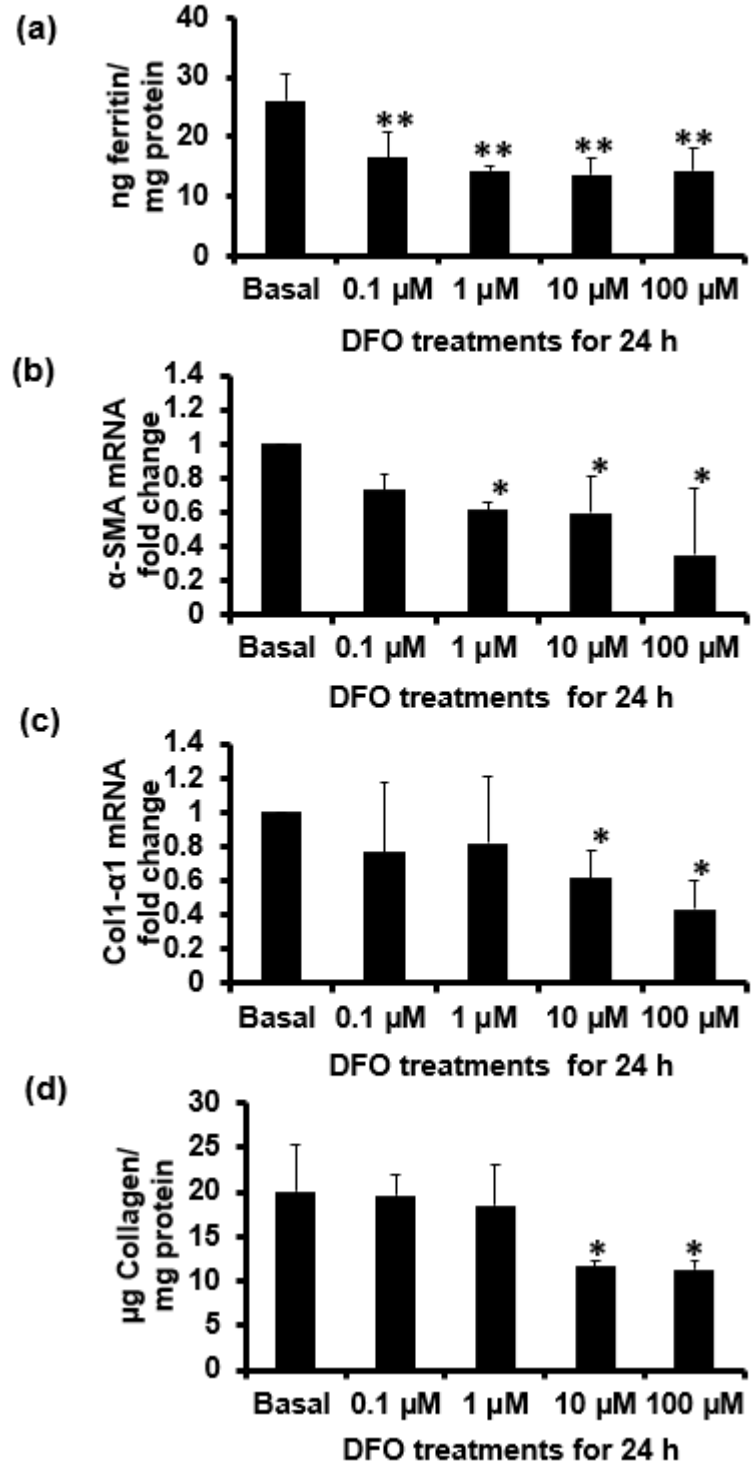
(a)
ng ferritin/ mg protein
40
30
20
10
0
**
**
**
**
Basal
0.1 μM
1 μM
10 μM
100 μM
DFO treatments for 24 h
(b)
α-SMA mRNA fold change
1.4
1.2
1
0.8
0.6
0.4
0.2
0
*
*
*
Basal
0.1 μM
1 μM
10 μM
100 μM
DFO treatments for 24 h
(c)
Col1-α1 mRNA fold change
1.4
1.2
1
0.8
0.6
0.4
0.2
0
*
*
Basal
0.1 μM
1 μM
10 μM
100 μM
DFO treatments for 24 h
(d)
μg Collagen/ mg protein
30
25
20
15
10
5
0
*
*
Basal
0.1 μM
1 μM
10 μM
100 μM
DFO treatments for 24 h

Fig.5

(a)

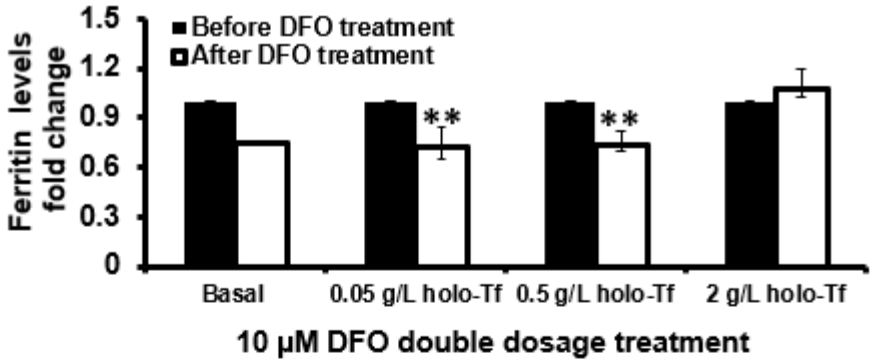
Before DFO treatment
After DFO treatment
Ferritin levels fold change
1.5
1.2
0.9
0.6
0.3
0
**
**
Basal
0.05 g/L holo-Tf
0.5 g/L holo-Tf
2 g/L holo-Tf
10 μM DFO double dosage treatment

(b)

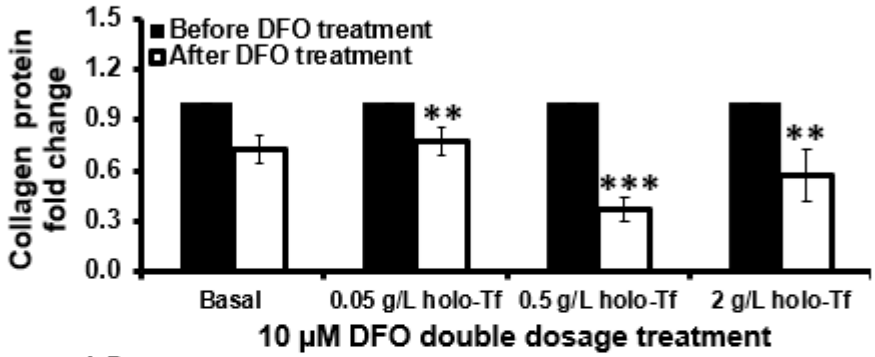
Before DFO treatment
After DFO treatment
Collagen protein fold change
1.5
1.2
0.9
0.6
0.3
0.0
**
***
**
Basal
0.05 g/L holo-Tf
0.5 g/L holo-Tf
2 g/L holo-Tf
10 μM DFO double dosage treatment

(c)

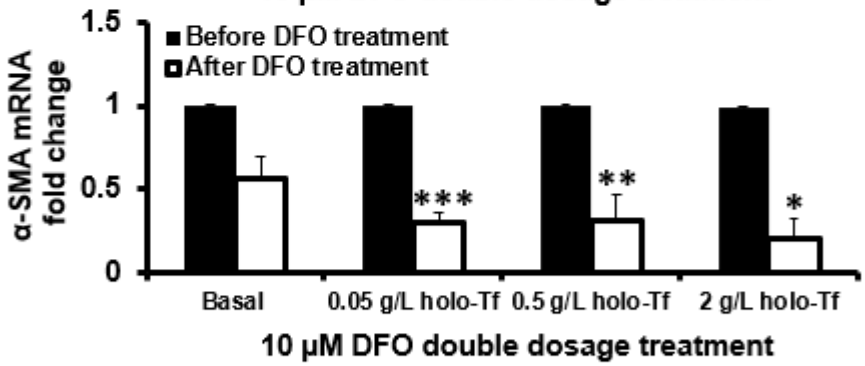
Before DFO treatment
After DFO treatment
α-SMA mRNA fold change
1.5
1
0.5
0
***
**
*
Basal
0.05 g/L holo-Tf
0.5 g/L holo-Tf
2 g/L holo-Tf
10 μM DFO double dosage treatment

(d)

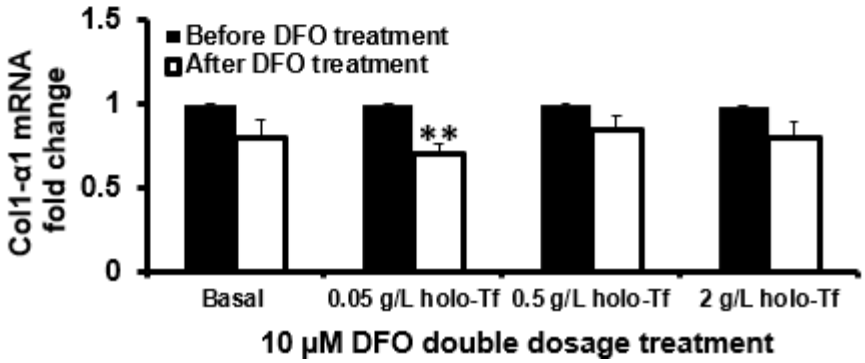
Before DFO treatment
After DFO treatment
Col1-α1 mRNA fold change
1.5
1
0.5
0
**
Basal
0.05 g/L holo-Tf
0.5 g/L holo-Tf
2 g/L holo-Tf
10 μM DFO double dosage treatment

Fig.6

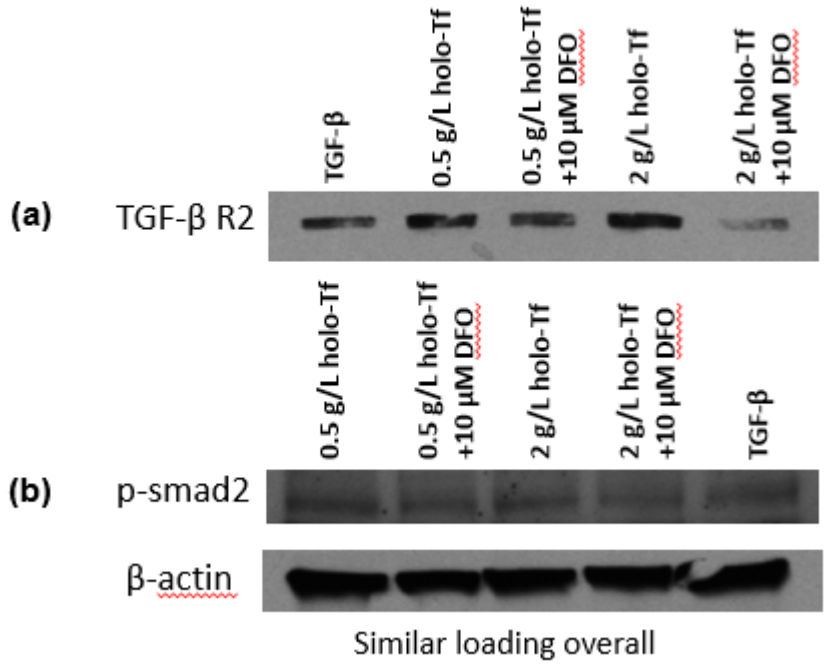
TGF-β
0.5 g/L holo-Tf
0.5 g/L holo-Tf +10 µM DFO
2 g/L holo-Tf
2 g/L holo-Tf +10 µM DFO
(a)
TGF-β R2
0.5 g/L holo-Tf
0.5 g/L holo-Tf +10 µM DFO
2 g/L holo-Tf
2 g/L holo-Tf +10 µM DFO
TGF-β
(b)
p-smad2
β-actin
Similar loading overall

Supplementary Table S1

Gene	Forward Primer 5’ to 3’	Reverse primer 5’ to 3’
Serpine-1	GCCAGATTTATCATCAATGACTGGG	GGAGAGGTGCACATCTTTCTCAAAG
Col1α1	AATGGCACGGCTGTGTGCGA	AGCACTCGCCCTCCCGTCTT
α-SMA	GCCAGTCGCTGTCAGGAACCC	AGCCCAGAGCCATTGTCGCA
TGF-β	GACAGCCCTGCTCACCGTCG	CCCGAGGGCTGGTCGGGAAT
Hif1-α	ACCTTCATCGGAAACTCCAAAG	CTGTTAGGCTGGGAAAAGTTAGG
Tfrc	TCATGAGGGAAATCAATGATCGTA	GCCCCAGAAGATATGTCGG
Slc40a1	TTGCAGGAGTCATTGCTGCTA	TGGAGTTCTGCACACCATTGAT
s9	AGCCGGCCTAGCGAGGTCAA	CGAAGGGTCTCCGTGGGGTCA

Supplementary Table S1: Primers for gene expression analysis

Primers for qRT-PCR analysis of fibrogenic and iron-related genes of interest are listed.

Supplementary Table S2

Protein	Primary antibody	Secondary antibody
TGF-β R II	Anti- TGF-β R II antibody (C-16): sc-220, rabbit polyclonal (Santa Cruz Biotechnology).	Anti-rabbit HRP conjugate 7074 P2 (Cell Signaling Technology)
phospho-Smad-2	Anti-Smad2 Antibody, phospho-specific (Ser465/467), AB3849, rabbit polyclonal (Abcam).	
Actin	AB75186, anti beta-actin loading control, rabbit polyclonal (Abcam).	
TfR1	Anti- transferrin receptor-1 antibody, AB84036. (Abcam).	
Vimentin	Anti-vimentin antibody, M7020, mouse monoclonal (Dako).	Anti-mouse HRP conjugate 7076 (Cell Signaling Technology)

Supplementary Table S2: Antibodies for western blot

Primary antibodies and the corresponding HRP- conjugated secondary antibodies used in the western blots are listed.

Supplementary Fig.1

(a)

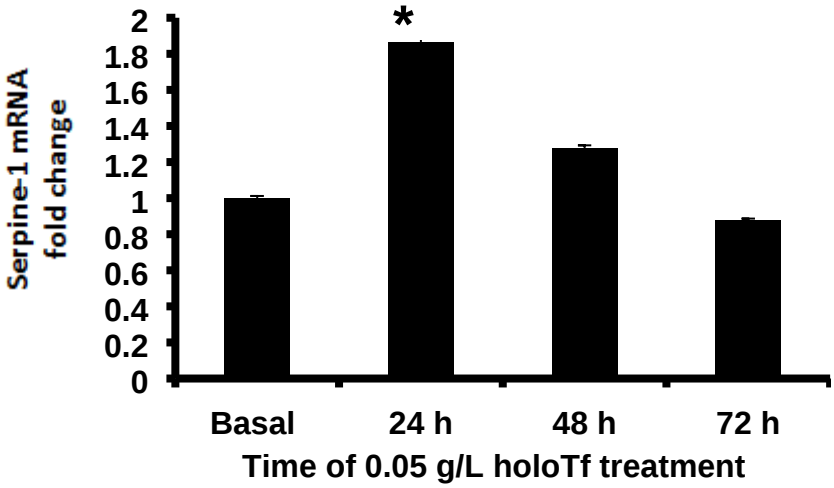

(b)

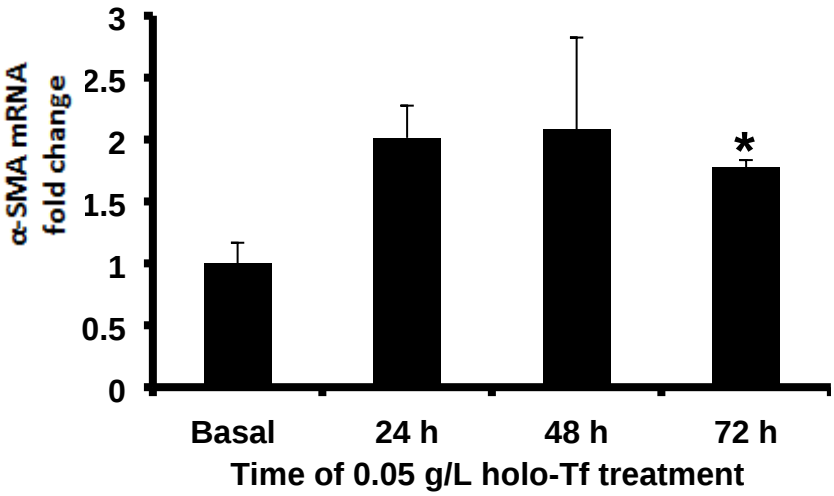

Supplementary Fig.1 Holo-Tf enhances HSC activation

The qRT-PCR detection of (a) Serpine-1 mRNA and (b) α-SMA mRNA are shown. Data is presented as mean ± SD. *p<=0.05 compared to basal conditions.

Supplementary Fig.2

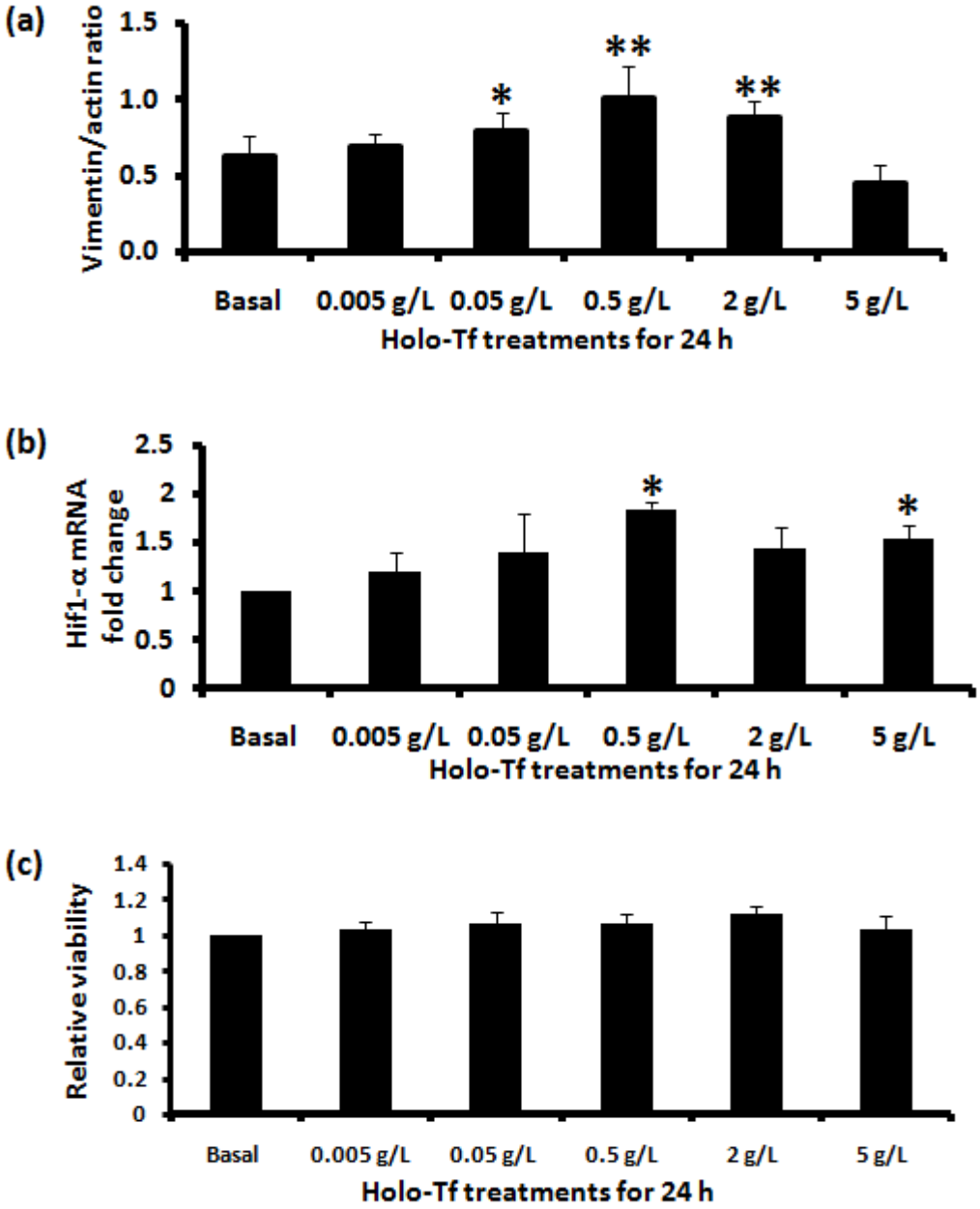

Supplementary Fig.2 Effect of holo-Tf on vimentin, Hif1-α mRNA and viability

(a) Density of vimentin protein bands, as analysed by the Image-J software following the detection by western blot. (b) qRT-PCR detection of Hif1-α mRNA and (c) cell viability following the treatments. Data is presented as mean ± SD. *p<0.05 and **p<0.01 compared to basal conditions.

Supplementary Fig.3

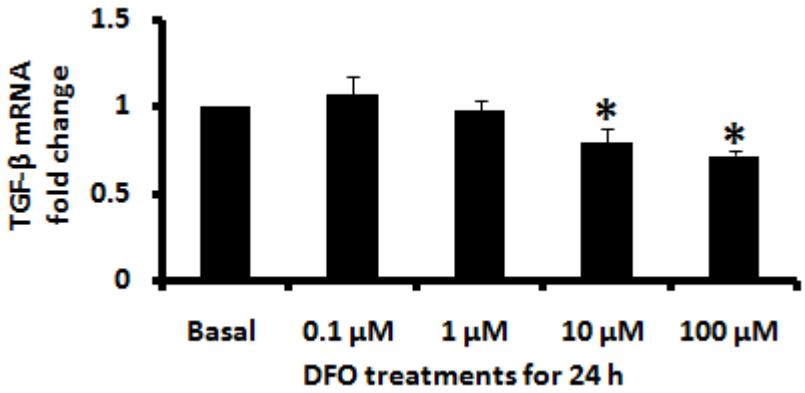

Supplementary Fig.3 Iron-chelation down-regulated *TGF-β* expression

Following treatments with a gradient of DFO concentrations, significant reduction in TGF-β mRNA was observed. Data is presented as mean ± SD. *p<0.05 compared to basal conditions.

Supplementary Fig.4

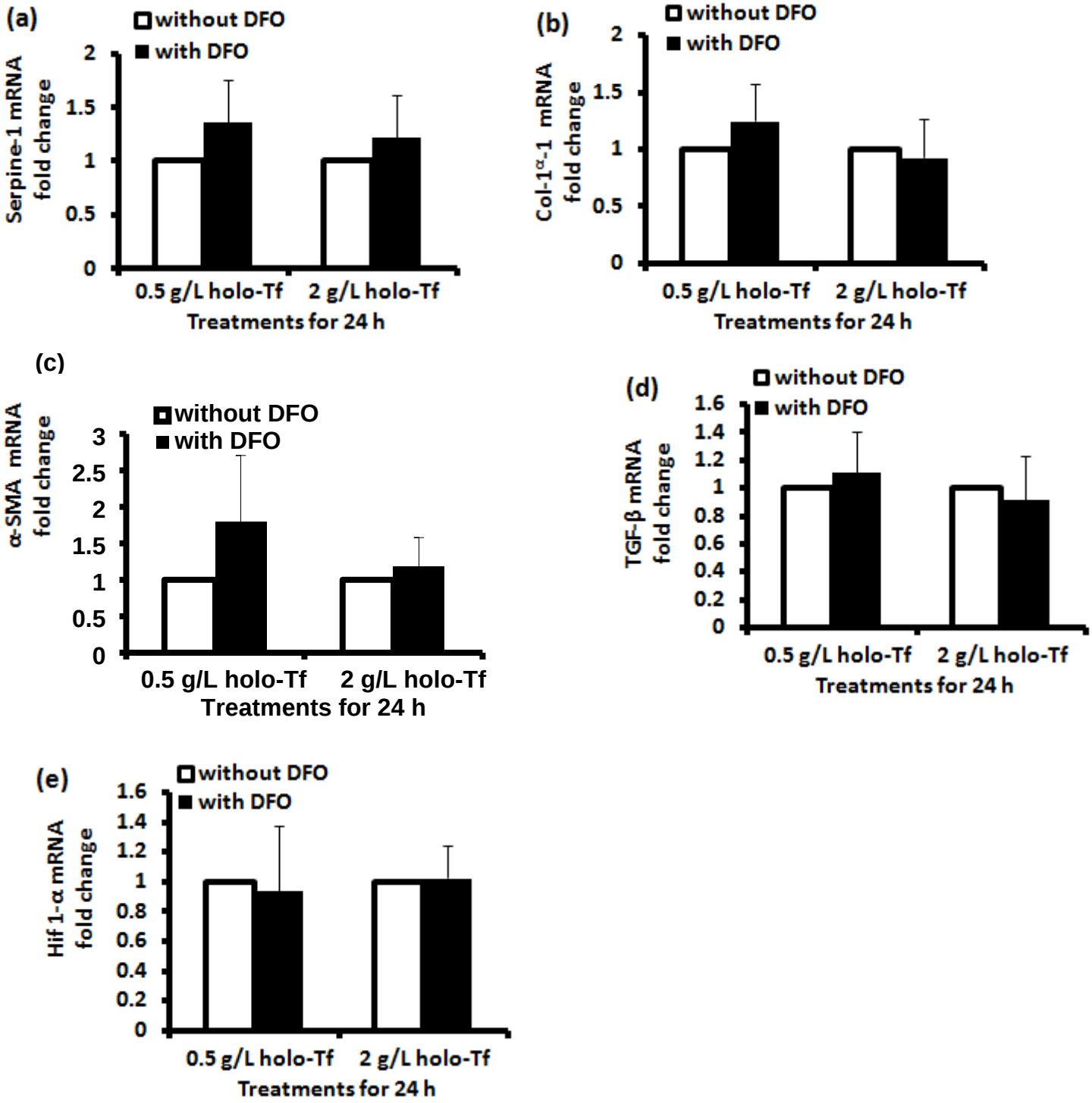

Supplementary Fig.4 Combined effect of holo-Tf and DFO on fibrogenic gene expression

The mRNA expression of (a) *serpine-1* (b) *Col1-α1* (c), *α-SMA* (d), *TGF-β* and (e) *Hif1-α* were studied following treatment with 10 µM DFO and 0.05 g/L or 2 g/L holo-Tf for 24 h. Data is presented as mean ± SD.

Supplementary Fig.5

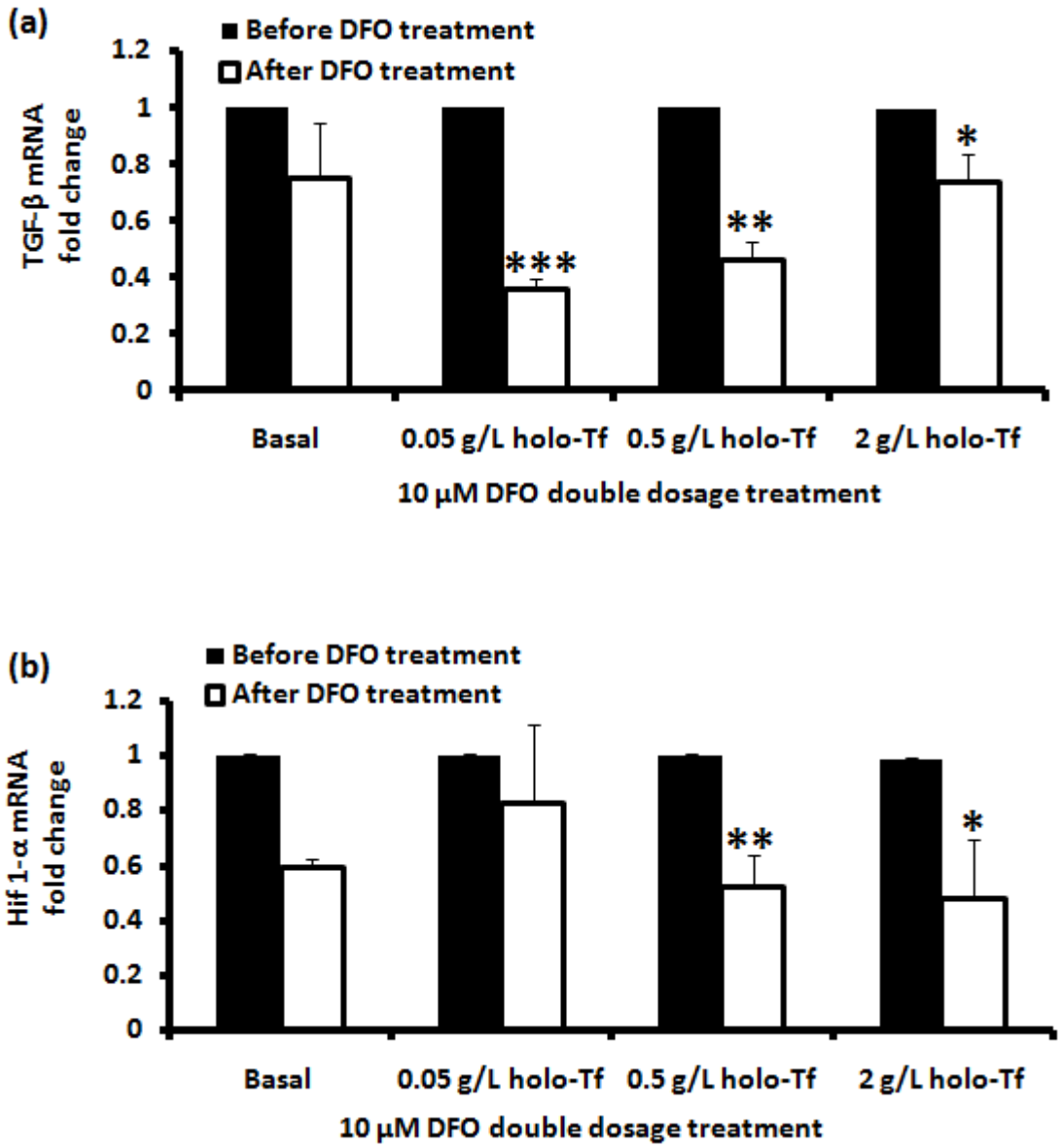

Supplementary Fig.5 Iron chelation attenuated the iron-induced expressions of *TGF-β* and *Hif1-α*

The qRT-PCR detection of (a) TGF-β mRNA and (b) Hif1-α mRNA following the DFO double dosage treatment (explained in Methods). Data is presented as mean ± SD. *p<=0.05, **p<0.03 and ***p<0.01compared to basal conditions.